

Full-Scale Testing of Deep Wide-Flange Steel Columns under Multiaxis Cyclic Loading: Loading Sequence, Boundary Effects, and Lateral Stability Bracing Force Demands

Ahmed Elkady, Ph.D., A.M.ASCE¹; and Dimitrios G. Lignos, A.M.ASCE²

Abstract: This paper discusses the findings from 10 full-scale steel column tests subjected to multiaxis cyclic loading. The columns use deep wide-flange cross sections typically seen in steel moment-resisting frames designed in seismic regions. The effects of boundary conditions, loading sequence, local web, and member slenderness ratios on the column hysteretic behavior are investigated. The test data underscore the influence of boundary conditions on the damage progression of steel columns. Local buckling followed by out-of-plane deformations near the plastified column base are the dominant failure modes in fixed base columns with a realistic flexible top end. Twisting may occur only at drifts larger than 3% even when the member slenderness is fairly large. The test data suggest that bidirectional loading amplifies the out-of-plane deformations but does not significantly affect the overall column performance. The loading sequence strongly affects the column's plastic deformation capacity but only at story drifts larger than 2%. Above this drift amplitude, column axial shortening grows exponentially and becomes a controlling failure mode. Measurements of the lateral stability bracing force demands at the column top exceed the lateral brace design force specified in North American standards. DOI: [10.1061/\(ASCE\)ST.1943-541X.0001937](https://doi.org/10.1061/(ASCE)ST.1943-541X.0001937). © 2017 American Society of Civil Engineers.

Author keywords: Deep steel columns; Boundary conditions; Full-scale tests; Column axial shortening; Out-of-plane brace force; Loading sequence; Plastic hinge length; Seismic effects.

Introduction

Because of their high moment of inertia to weight ratio, deep and slender wide-flange steel columns [i.e., depth $d \geq 400$ mm (16 in.)] represent an economical solution for the seismic design of modern steel moment-resisting frames (MRFs). The term slender refers to deep cross sections that are seismically compact and whose web and flange slenderness ratios are within the seismic compactness limits for highly ductile members (λ_{hd}) as per AISC (2010a).

Past experimental studies on fully restrained beam-to-column moment connections that used deep columns (Chi and Uang 2002; Ricles et al. 2004) demonstrated that such members could be susceptible to twisting. This is exacerbated by the torsional demand and out-of-plane bending imposed on the column because of the inelastic buckling of the steel beam protected zones. Surveys from past full-scale experiments (FEMA 2000; Lignos and Krawinkler 2011, 2013) suggest that deep and slender wide-flange beams (i.e., in the absence of compressive axial load) deteriorate in flexural strength and stiffness at story drift ratios on the order of 2.5% on average. This is due to the early onset of geometric instabilities (e.g., web and flange local buckling). Detailed finite-element studies (Elkady and Lignos 2012, 2013, 2015a; Fogarty and El-Tawil 2015) associated with the

cyclic behavior of steel columns of similar-size cross sections indicate that this issue becomes more critical in the presence of compressive axial loads. Notably, NIST (2010b) developed a research plan that aimed for a comprehensive understanding of the seismic behavior of deep and slender wide-flange columns and the development of guidelines for the seismic design of such members.

Early experimental studies on steel wide-flange columns mostly used relatively small cross sections with depths ranging from W4 to W10 (Popov et al. 1975; MacRae et al. 1990; Nakashima et al. 1990). These specimens were tested either as cantilevers or with fixed-end boundaries (noted as fixed-fixed from this point on). Therefore, the location of the inflection point was constant throughout the loading sequence. The focus of these tests was primarily on the effects of local slenderness on the hysteretic behavior of steel columns. These testing programs revealed that (1) column axial shortening is a critical failure mode that influences the steel column stability (MacRae et al. 1990, 2009); and (2) cyclic deterioration in the column's flexural strength becomes severe when subjected to compressive axial load levels larger than 50% of the column's axial yield strength, P_y (Popov et al. 1975). More recently, Newell and Uang (2008) tested, at full-scale, steel columns with stocky W14 cross sections in a fixed-fixed configuration. These members were able to sustain story-drift ratios of 7% prior to 10% reduction in their flexural strength, even at high axial load demands. Notably, Ozkula et al. (2017) conducted full-scale tests on steel columns with deep and slender wide-flange cross sections and fixed-fixed boundary conditions. These tests revealed that the observed failure modes might vary between local and lateral torsional buckling depending on the local and member slenderness ratios.

The previously mentioned experimental studies share the following limiting features:

1. They were primarily conducted with simplified boundary conditions (i.e., cantilever or fixed-fixed); in this case, the

¹Postdoctoral Research Scientist, Swiss Federal Institute of Technology, Ecole Polytechnique Federale de Lausanne, 1015 Lausanne, Vaud, Switzerland.

²Associate Professor, Swiss Federal Institute of Technology, Ecole Polytechnique Federale de Lausanne, 1015 Lausanne, Vaud, Switzerland (corresponding author). E-mail: dimitrios.lignos@epfl.ch

Note. This manuscript was submitted on February 11, 2017; approved on July 10, 2017; published online on November 17, 2017. Discussion period open until April 17, 2018; separate discussions must be submitted for individual papers. This paper is part of the *Journal of Structural Engineering*, © ASCE, ISSN 0733-9445.

torsional rigidity at the member ends was simultaneously lost after the formation of flexural yielding and the onset of local buckling. This strongly influences global failure modes associated with plastic lateral torsional buckling (Galambos and Surovek 2008).

2. The effects of bidirectional loading because of three-dimensional ground motion shaking were neglected.
3. The influence of the loading history on the column hysteretic behavior was not assessed.
4. The lateral stability bracing force demands at the columns' top boundary was never quantified such that the lateral bracing requirements in such members can be evaluated.

To address these issues, this paper presents a comprehensive full-scale testing program that investigated the hysteretic behavior of 10 deep and slender wide-flange steel columns subjected to multiaxis cyclic loading. The focus is on first-story interior columns in multistory steel MRFs designed in highly seismic regions. More specifically, the scope and objectives of this paper are as follows:

1. To assess the effects of cross-section slenderness and its interaction with member slenderness on steel column stability. Emphasis is placed on the plastic hinge length formation and the local and member instabilities observed during the damage progression.
2. To examine the effects of column end boundary conditions and lateral loading histories on the cyclic behavior of steel columns.
3. To quantify the influence of bidirectional loading histories on the steel column stability.
4. To quantify the lateral stability bracing forces developed at the top end of steel columns and to assess the current North American design requirements for lateral bracing of steel columns.

Specific performance indicators of interest are the steel column axial shortening, member out-of-plane deformations, and flexural strength and stiffness deterioration at story-drift ratios of interest to the engineering profession.

Description of the Test Setup

The test program was conducted at the structures laboratory of École Polytechnique de Montréal with a six-degree-of-freedom test setup as shown in Fig. 1. This setup comprises a steel base plate anchored to the laboratory's strong floor and a steel top platen connected to four vertical actuators. A pair of horizontal actuators per loading direction is connected to the top platen. Referring to Fig. 1, these actuators provide full control of the six degrees of freedom (DOF) ($\delta_x, \delta_y, \delta_z, \theta_x, \theta_y, \theta_z$) at the top platen with mixed displacement and force control. The test setup allows for the realistic representation of the boundary conditions seen in first-story steel MRF columns because of the flexibility of the beam-to-column connections intersecting a column. In this case, the inflection point location is not fixed but moves while the plasticification progresses in the column. To the best of the authors' knowledge, this has never been investigated in prior studies. In order to facilitate the discussion in the subsequent sections, the reference coordinate system X–Y–Z, shown in Fig. 1, is used.

Description of the Test Matrix

Cross Sections

Table 1 provides an overview of the test matrix in terms of the selected cross sections, applied lateral loading history and compressive axial load ratio, and boundary conditions. The test matrix comprises 10 column specimens (labeled C1–C10) in total. This includes six and four nominally identical column specimens that

use a W24×146 and a W24×84 cross section, respectively. The former is commonly found in first-story columns in modern low- and mid-rise steel MRFs designed in North America (NIST 2010a; Elkady and Lignos 2014, 2015b). The latter is representative of columns in low-rise steel special moment frames (SMFs), ordinary steel MRFs, and multitiered braced frames (Stoakes and Fahnstock 2016). Table 1 summarizes the measured geometric properties of the two selected cross sections. Both cross sections have the same flange slenderness ratio ($b_f/2t_f = 6.0$, where b_f is the flange width; and t_f is the flange thickness of the cross section) but different web slenderness ratios [$h/t_w = 33$ and 47.3 for the W24×146 and W24×84 cross sections, respectively; t_w is the web thickness; and h is the clear web height as defined in AISC (2010a)]. In this way, we can assess the influence of h/t_w on the column hysteretic behavior. Detailed finite-element studies (Elkady and Lignos 2013) prior to the testing program indicated that the web slenderness controls the column response over the flange slenderness. The web and flange slenderness ratios of the selected cross sections comply with the compactness limits for highly ductile members (λ_{hd}) as per AISC (2010a). The W24×84 column has a member slenderness ratio, $L_b/r_y = 79$ (L_b is the laterally unsupported length; and r_y is the radius of gyration about the cross section's weak axis). For the W24×146 column, $L_b/r_y = 51$. This ratio influences the column hysteretic response when member geometric instabilities are triggered. The member slenderness ratios of the selected column cross sections allow for the assessment of the $L_b/r_y \approx 60$ limit specified by the Canadian seismic provisions (CSA 2009). Referring to Table 1, the plastic moment (M_p)-to-elastic critical moment (M_{cr}) ratio (i.e., torsional slenderness ratio, λ_{LTB}) indicates how susceptible a column may be to lateral torsional buckling.

The column specimens have a clear length $L = 3,900$ mm (approximately 13 ft). Each cross section is welded into two 75-mm thick steel plates with complete joint penetration (CJP) J-groove welds. Weld access holes are prepared according to Section J1.6 of the AISC steel specifications (AISC 2010b). The column specimens are fabricated from A992 Grade-50 steel (i.e., nominal yield stress $f_{yN} = 345$ MPa) as per ASTM (2015). Rectangular tensile coupon specimens are cut from the cross-section web and flanges to obtain their material properties in accordance with ASTM (2014). Table 1 summarizes the web and flange average material properties based on three tensile coupon tests per location. Specimens C1–C4, C5 and C6, and C7–C10 are fabricated by three different steel batches. The three steel materials have a similar carbon equivalent value of 0.35%, which complies with the maximum permissible level of 0.45% specified by ASTM (2015).

Loading Protocols

The focus of this paper is on interior columns because their hysteretic behavior is deemed more critical than that of end columns (Suzuki and Lignos 2014, 2015). In particular, end columns experience large axial load demand fluctuations because of the dynamic overturning effects; hence, the neutral axis within the column cross section considerably shifts while the axial load varies from compressive to tensile axial load demands coupled with lateral drift deformations. Therefore, the column axial shortening does not accumulate compared to interior columns in which the compressive axial load remains more or less constant (Suzuki and Lignos 2014, 2015).

To this end, nine out of ten specimens are subjected to a constant compressive axial load, $P = 20\%P_y$. Although this depends on the building plan view and lateral load resisting frame configuration, $P/P_y = 20\%$ is very representative of modern steel-frame

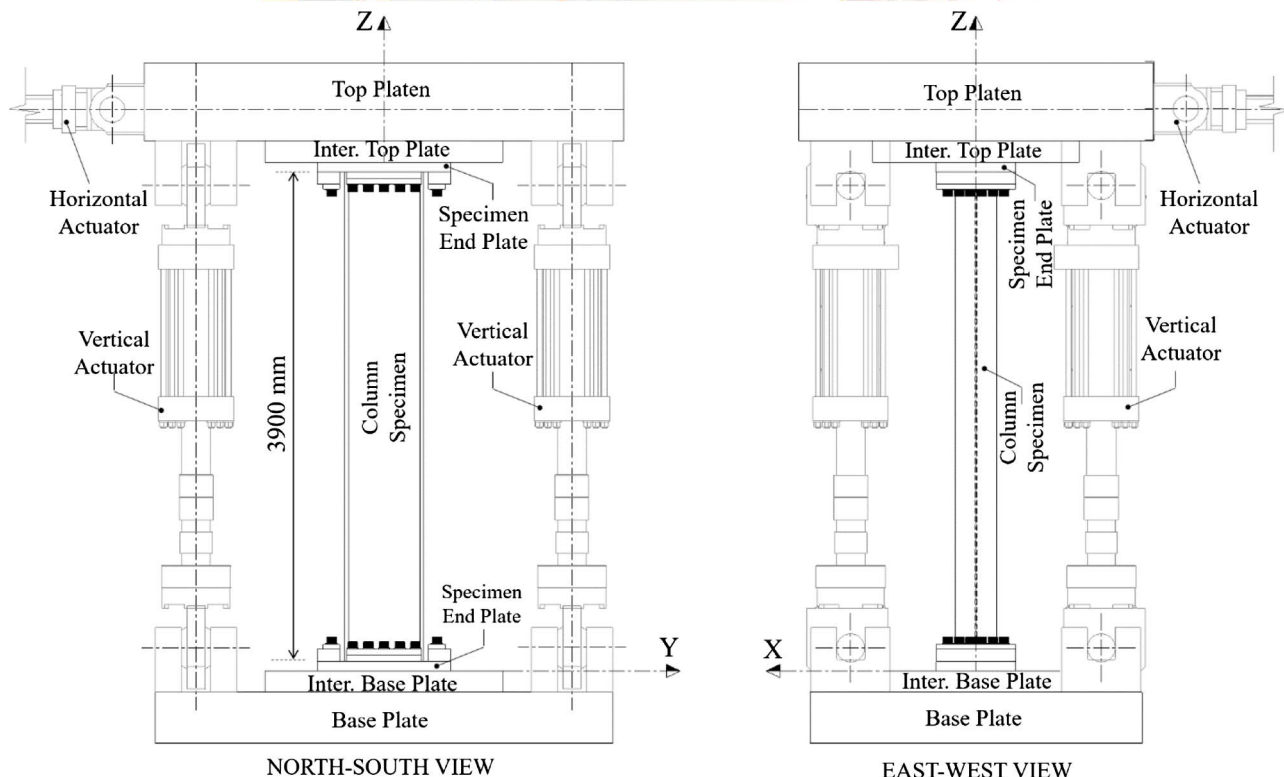
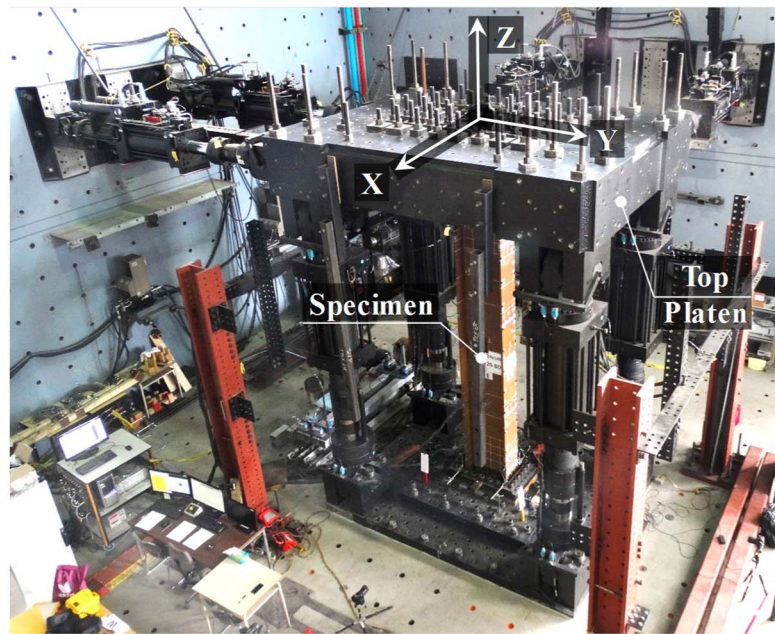


Fig. 1. Description of the six-DOF test setup at École Polytechnique de Montréal

buildings with SMFs (NIST 2010a; Elkady and Lignos 2014, 2015b). The same axial load ratio complies with the upper limit of 30% P_y according to the Canadian seismic provisions (CSA 2009) for Type-D ductile steel MRFs. The AISC (2010a) seismic provisions do not consider such a limit for steel SMFs. In order to examine the influence of high compressive axial load demands on the steel column hysteretic behavior, one specimen (Specimen C2) is subjected to 50% P_y (i.e., $P/P_{cl} \approx 60\%$, where P_{cl} lower-bound axial strength of a steel column as per ASCE 41-13). This is representative of interior steel columns in 1970s tall steel MRF buildings (Bech et al. 2015). Therefore, Specimen C2 offers the opportunity to examine if steel columns that exhibit high compressive

axial load coupled with lateral drift demands should be treated as force-controlled elements as per ASCE 41-13 (ASCE 2014).

Referring to Table 1, two types of unidirectional (UD) lateral-loading protocols are used. The first is the standard symmetric cyclic (noted here as “SYM”) lateral-loading protocol (Clark et al. 1997). This protocol is shown in Fig. 2(a) and has been routinely used in past experimental studies (e.g., FEMA 2000). The second one is a collapse-consistent lateral-loading protocol (noted here as “CPS”) developed by Suzuki and Lignos (2014, 2015). Referring to Fig. 2(b), this protocol involves few inelastic lateral-loading cycles followed by large monotonic pushes in one direction (“ratcheting”) (Ibarra and Krawinkler 2005). This is representative

Table 1. Test Matrix Summary and Measured Geometric and Material Properties

Identifier	Section size	Lateral-loading protocol	$\frac{P}{P_y}$	BCs in the strong-axis direction	Cross section and member properties							Measured material properties ^a			
					b_f	h	L_b	J (mm ⁴)	C_w (mm ⁶)	λ_{LTB}	E (MPa)	Flange		Web	
					$2t_f$	t_w	r_y					f_{yf}	f_{uf}	f_{yw}	f_{uw}
C1	W24×146	SYM (UD)	-0.2	Fixed-fixed	6.1	33.3	51.7	5.1×10^6	1.4×10^{13}	0.28	190,481	414	509	415	502
C2	W24×146	SYM (UD)	-0.5	Fixed-fixed	6.1	33.1	51.5	5.1×10^6	1.4×10^{13}	0.28	190,481	414	509	415	502
C3	W24×146	SYM (UD)	-0.2	Fixed-flexible	6.1	33.5	51.5	5.0×10^6	1.4×10^{13}	0.32	190,481	414	509	415	502
C4	W24×146	CPS (UD)	-0.2	Fixed-flexible	6.1	33.3	51.7	5.1×10^6	1.4×10^{13}	0.28	190,481	414	509	415	502
C5	W24×146	CPS (UD)	-0.2	Fixed-flexible	6.0	32.5	52.1	5.2×10^6	1.4×10^{13}	0.30	204,413	368	483	378	479
C6	W24×146	SYM (BD)	-0.2	Fixed-flexible	5.9	32.2	52.3	5.3×10^6	1.4×10^{13}	0.30	204,413	368	483	378	479
C7	W24×84	SYM (UD)	-0.2	Fixed-flexible	6.1	47.0	79.2	1.6×10^6	3.3×10^{13}	0.42	195,203	332	507	345	508
C8	W24×84	CPS (UD)	-0.2	Fixed-flexible	6.1	47.0	79.2	1.6×10^6	3.3×10^{13}	0.42	195,203	332	507	345	508
C9	W24×84	SYM (BD)	-0.2	Fixed-flexible	6.1	47.7	79.4	1.5×10^6	3.2×10^{13}	0.42	195,203	332	507	345	508
C10	W24×84	CPS (BD)	-0.2	Fixed-flexible	6.1	47.4	79.6	1.5×10^6	3.3×10^{13}	0.42	195,203	332	507	345	508

Note: b_f = flange width; C_w = warping constant; E = elastic modulus; f_{uf} = flange ultimate stress; f_{uw} = web ultimate stress; f_{yf} = flange yield stress; f_{yw} = web yield stress; h = web height; J = torsion constant; t_w = web thickness; t_f = flange thickness.

^a $\lambda_{LTB} = (Z_x f_y / M_{cr})^{0.5}$; $M_{cr} = C_1 \pi^2 EI_y / (k_y L)^2 [C_w / I_y (k_y / k_w)^2 + GJ (k_y L_e)^2 / (\pi^2 EI_y)]^{0.5}$, where $k_w = 1.0$, $k_y = 0.5$, and $C_1 = 2.76$ and 2.08 for fixed-fixed and fixed-flexible specimens, respectively.

of what a first-story column would experience when a building is subjected to a low probability of occurrence seismic event (Lignos et al. 2011, 2013).

Bidirectional (BD) cyclic symmetric and collapse-consistent loading protocols (noted as "SYM-BD" and "CPS-BD," respectively) are also used. These involve elliptical drift cycles in the XY plan view as shown in Figs. 2(c and d) for the SYM-BD and CPS-BD protocols, respectively. These protocols were developed based on concepts discussed in Krawinkler (1996, 2009). In brief, the SYM-BD lateral protocol reaches a maximum drift ratio of 2% in the column's weak-axis bending direction during the 3% drift amplitude cycle in the column's strong-axis bending direction. Similarly, the CPS-BD lateral-loading protocol reaches a maximum drift ratio of 3% in the X-loading direction during the first excursion of the 5% drift amplitude in the Y-loading direction. Further details regarding the development of these protocols can be found in Elkady (2016).

Boundary Conditions

Specimens C1 and C2 are tested with fixed-end boundaries in the strong-axis bending direction. The rest of the specimens are tested with a fixed base and a flexible top end boundary (noted as fixed-flexible). To simulate the flexible boundary conditions, a predefined rotation, R_x , is applied about the x-axis at the specimen top end. This rotation history is synchronized with the lateral drift in the y-axis direction. The predefined rotation is such that the inflection point within the column is set at $0.75L$ from the column base prior to column plastification. The inflection point location is chosen based on surveys from numerous studies on the seismic behavior of typical steel MRFs ranging from 1 to 20 stories and 1 to 5 bays, conducted by the authors as well as others (Gupta and Krawinkler 1999; Lignos et al. 2010; NIST 2010a; Suzuki and Lignos 2014; Elkady and Lignos 2015b). All specimens are assumed to be fixed in their weak-axis bending direction including the torsional degrees of freedom. This assumption may not be necessarily true for the column top end once local buckling initiates at

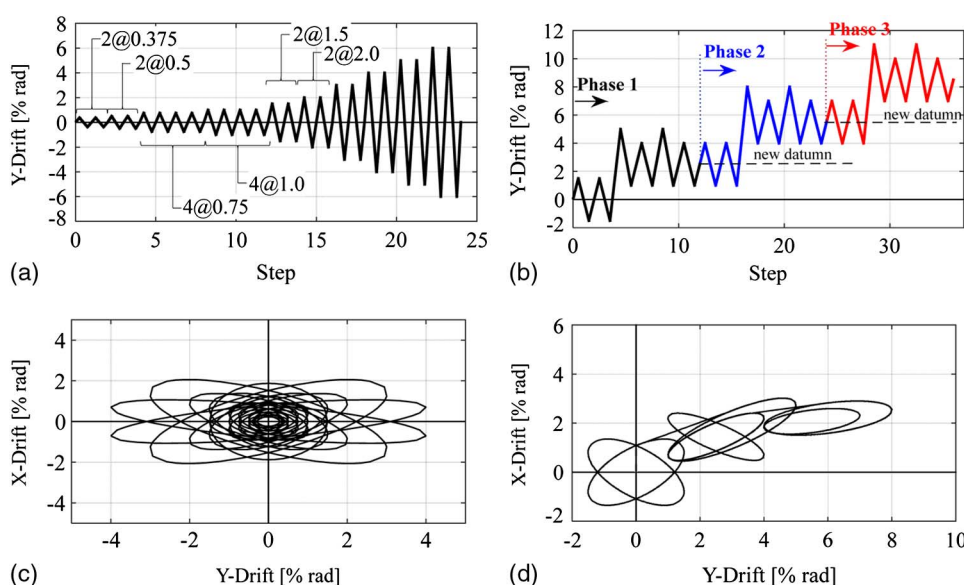


Fig. 2. Lateral-loading protocols used in the experimental program: (a) unidirectional symmetric protocol; (b) unidirectional collapse-consistent protocol; (c) bidirectional symmetric protocol; (d) bidirectional collapse-consistent protocol

the adjoining steel beams. Depending on the beam-to-column connection type, an appreciable amount of torsional force may be applied to the steel column (Chi and Uang 2002; Zhang and Ricles 2006). This issue deserves more attention in future research studies.

Qualitative Summary of Typical Steel Column Damage Progression

The typical damage progression sequence leading to a loss of flexural or axial load-carrying capacity of a steel column is shown in Figs. 3(a–i) and 4(a–i). Referring to Fig. 3, the end moment is normalized with respect to the measured full plastic flexural strength M_p without any reduction because of the applied compressive axial load. The deduced end moment at any load increment is computed as the summation of the actuator force components transformed to the global coordinate system (Fig. 1) multiplied by the corresponding distance from the actuator swivel to the column base or top. In Fig. 3, the true chord rotation is calculated over the test specimen's length after subtracting the measured column axial shortening. This represents the story-drift-ratio demands that a column experiences under reversed cyclic loading. Results for Specimen C4 are disregarded because of a control error in the loading rate application of the rotational DOF (R_x).

Fig. 5 shows the applied lateral-loading protocol for Specimen C7 in the strong-axis bending direction including key damage

states. The initial elastic cycles did not induce any notable deformation in the specimen. Flexural yielding occurred in the web and flanges prior to the 1.5% drift amplitude. From Fig. 6(a), the inflection point was located near $0.75L$ from the column base as intended. Referring to Fig. 3(f), prior to the onset of local buckling, Specimen C7 reached a maximum flexural strength, M_{\max} , which was 10% higher than its expected unreduced plastic flexural capacity (i.e., $M_{\max}/M_p = 1.1$). Referring to Fig. 3, the same amount of cyclic hardening was observed in all the test specimens subjected to a $P/P_y = 20\%$.

Referring to Fig. 7(a), flange and web local buckling near the column base became evident at the first cycle of the 2% drift amplitude and progressed during larger amplitude loading cycles. The center of the flange local buckling wave was located at $0.6d$ from the bottom end plate. From Fig. 7(b), the local buckling formation was fairly symmetric because of the imposed loading history. This was not the case for specimens subjected to a collapse-consistent loading history in which local buckling was only evident on the compressive flange due to ratcheting. Local buckling triggered flexural and axial strength deterioration near the column base [Figs. 3(f) and 4(f)]. This caused the inflection point to move toward the column base as shown in Fig. 6(a). This was due to the force redistribution within the column once flexural strength deterioration initiated at the column base. Referring to Fig. 6(b), this was also observed in Specimen C8, which was subjected to

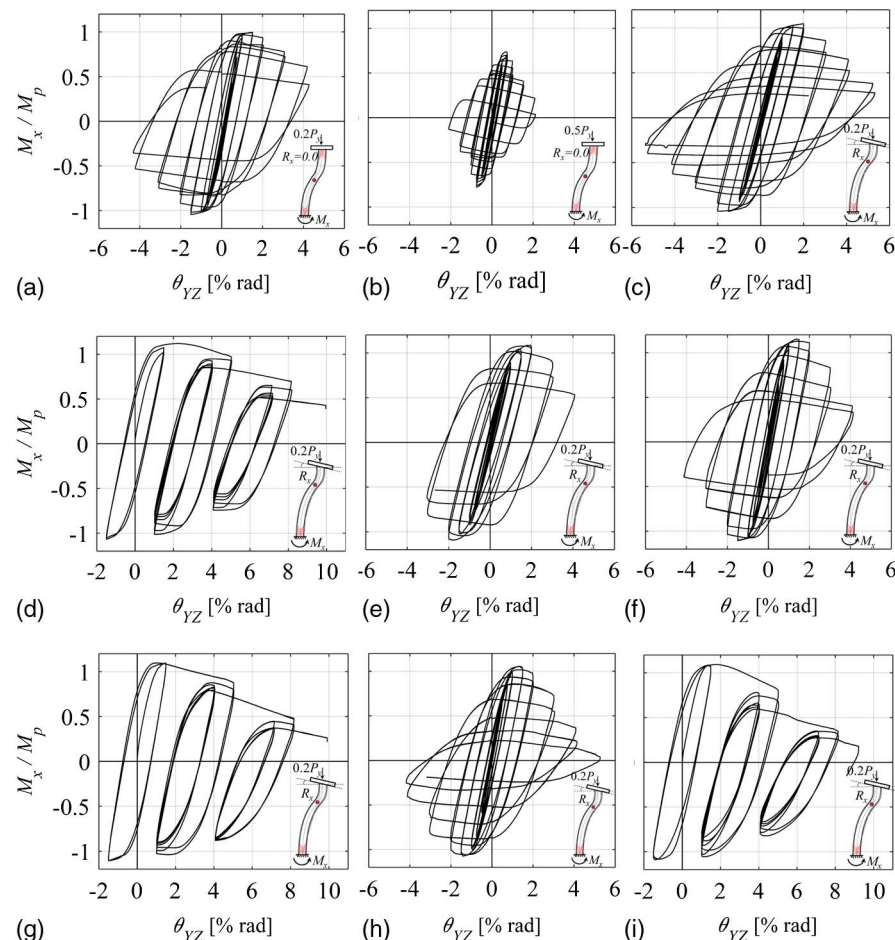


Fig. 3. Normalized column base end moment versus true chord rotation in the strong-axis direction: (a) Specimen C1 (W24×146, SYM-UD-0.2Py); (b) Specimen C2 (W24×146, SYM-UD-0.5Py); (c) Specimen C3 (W24×146, SYM-UD-0.2Py); (d) Specimen C5 (W24×146, CPS-UD-0.2Py); (e) Specimen C6 (W24×146, SYM-BD-0.2Py); (f) Specimen C7 (W24×84, CPS-UD-0.2Py); (g) Specimen C8 (W24×84, CPS-UD-0.2Py); (h) Specimen C9 (W24×84, SYM-BD-0.2Py); (i) Specimen C10 (W24×84, CPS-BD-0.2Py)

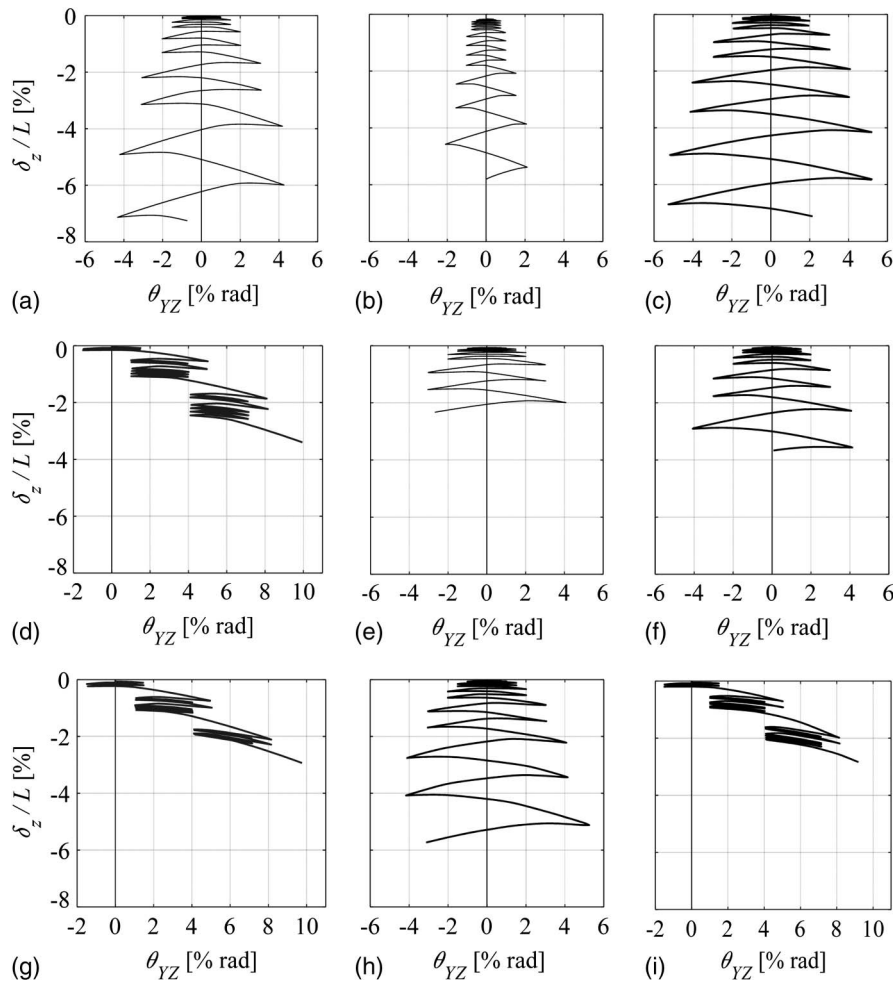


Fig. 4. Normalized column axial shortening versus true chord rotation in the strong-axis direction: (a) Specimen C1 (W24×146, SYM-UD-0.2Py); (b) Specimen C2 (W24×146, SYM-UD-0.5Py); (c) Specimen C3 (W24×146, SYM-UD-0.2Py); (d) Specimen C5 (W24×146, CPS-UD-0.2Py); (e) Specimen C6 (W24×146, SYM-BD-0.2Py); (f) Specimen C7 (W24×84, CPS-UD-0.2Py); (g) Specimen C8 (W24×84, CPS-UD-0.2Py); (h) Specimen C9 (W24×84, SYM-BD-0.2Py); (i) Specimen C10 (W24×84, CPS-BD-0.2Py)

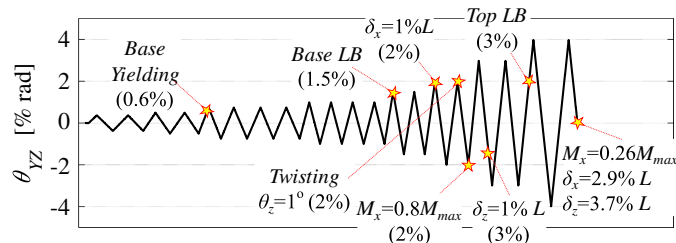


Fig. 5. Applied drift history in the strong axis for Specimen C7 with key damage states indicated

a collapse-consistent loading protocol. Notably, the force redistribution was not evident in fixed-end test specimens; thus, the inflection point remained at the column midheight because of the simultaneous plastification of its ends [Fig. 6(c) for Specimen C1].

Web local buckling caused column axial shortening, which in turn triggered considerable out-of-plane global deformations in specimens with fixed-flexible boundary conditions as shown in Fig. 8. The same figure shows the magnitude and progression of these out-of-plane deformations as monitored by a wireless

displacement tracking system. Such deformations caused appreciable weak-axis moment demands because of member P-delta forces (i.e., $M_{y,P-Delta} = P\delta_x$). For instance, for Specimen C7 [Fig. 8(a)], at the 4% drift amplitude with respect to the strong-axis bending, the weak-axis moment demands were equal to approximately 60% of the column's weak-axis plastic flexural strength (i.e., $M_{y,P-Delta} = 0.6M_{p,y}$). This observation holds true for all the specimens tested with fixed-flexible boundary conditions, regardless of the lateral-loading protocol used. Notably, this is not traced when columns are tested with fixed-fixed boundary conditions [Fig. 8(c)].

Finally, the out-of-plane deformations were followed by column twisting near the specimen's base. The cross-section twisting angle (θ_z) was quantified using six string potentiometers attached to both flanges at three cross-sectional levels ($1/4 L$, $1/2 L$, and $3/4 L$) as well as the wireless displacement tracking system. Fig. 9 shows the cross-section twist angle versus chord rotation for Specimen C7. Although in this case, $L_b/r_y = 79$, the column twisting became evident near the column base (i.e., at $1/4 L$) only after the 3% drift amplitude. By the end of the test, the maximum twisting angle was approximately 3.5° near the column base plastic hinge region but less than 1° near the column top end. This was because the torsional restraint at the column top was not lost simultaneously with that of the column base after the onset of local buckling. This indicates that characterizing the hysteretic behavior of steel columns with

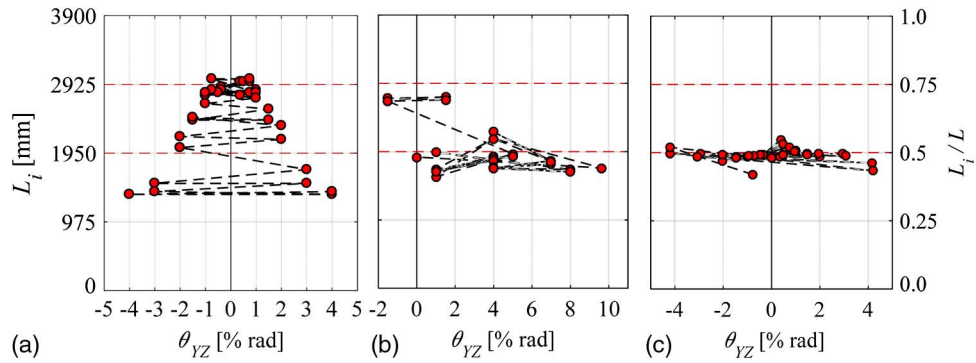


Fig. 6. Inflection point location history for specimens with various boundary conditions: (a) Specimen C7 (fixed-flexible, SYM-UD); (b) Specimen C8 (fixed-flexible, CPS-UD); (c) Specimen C1 (fixed-fixed, SYM-UD)

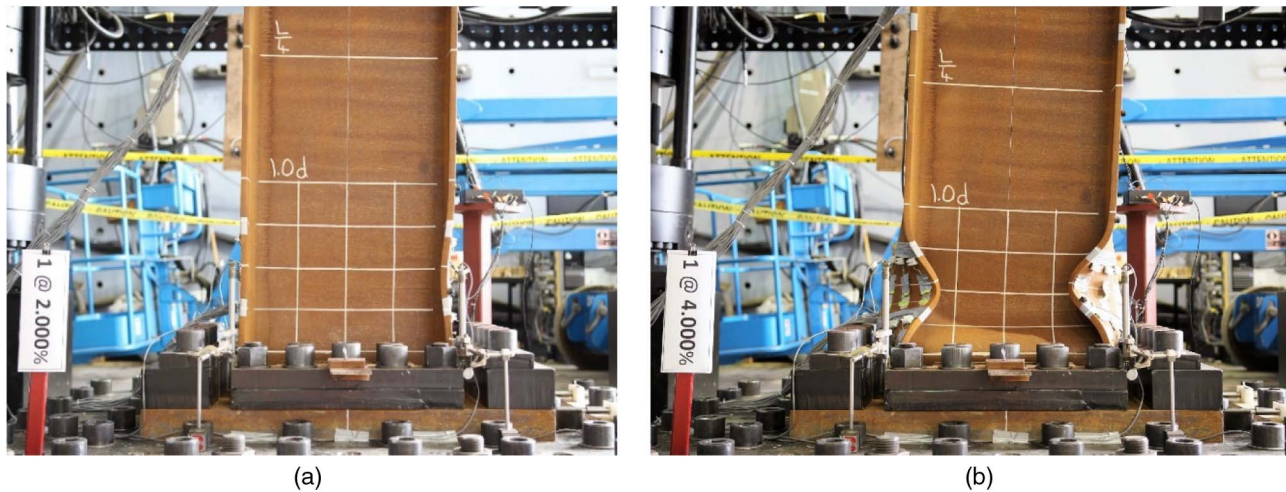


Fig. 7. Local buckling progression near the base of Specimen C7: (a) first cycle, 2% drift amplitude; (b) first cycle, 4% drift amplitude

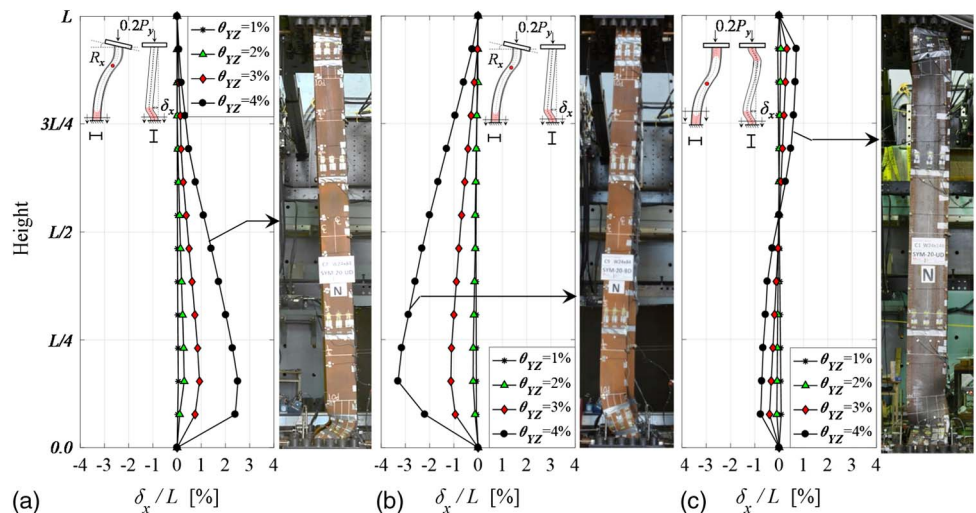


Fig. 8. Out-of-plane deformation profiles at selected drift amplitudes for selected specimens: (a) Specimen C7 (fixed-flexible, SYM-UD); (b) Specimen C9 (fixed-flexible, SYM-BD); (c) Specimen C1 (fixed-fixed, SYM-UD)

simplified fixed-fixed boundary conditions may be misleading. This is further elaborated in the subsequent sections.

Referring to Fig. 3(f), because of the observed out-of-plane deformations and the associated twisting, Specimen C7 lost more than

70% of its initial lateral stiffness (K_e) near its base. Furthermore, referring to Fig. 4(f), the same specimen shortened by 145 mm (3.7% L) at the end of the test. At this point, its flexural capacity was reduced by more than 70% M_{max} [Fig. 3(f)].

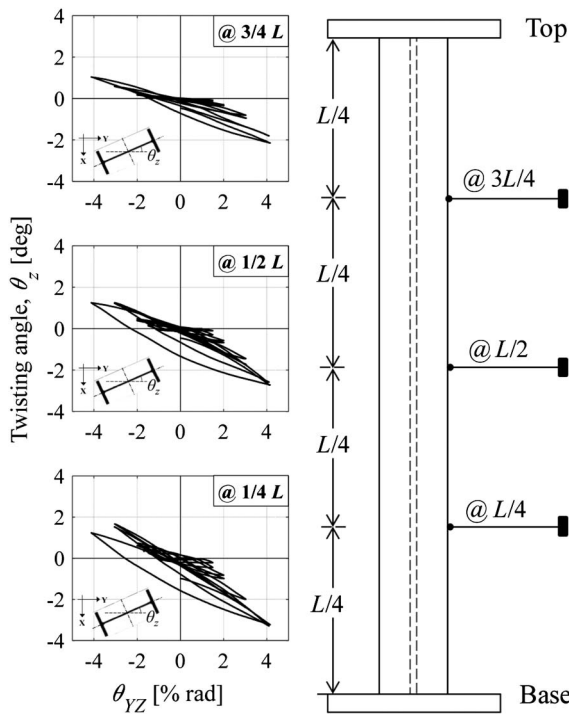


Fig. 9. Twisting angle versus true chord rotation at different cross-sectional levels of Specimen C7

Synthesis of Experimental Results and Discussion

This section provides a synthesis of the experimental data to assess several aspects related to the steel column stability due to reversed cyclic loading.

Effect of Cross Section and Member Slenderness

Referring to Figs. 3 and 4, steel column flexural and axial strength deterioration, unloading stiffness deterioration, and column axial shortening were primarily induced by the interactive effects of local buckling and out-of-plane deformations. To assess the influence of the cross-section web and member slenderness on the hysteretic behavior of steel columns, three pairs of specimens are compared: Specimens C3 and C7; Specimens C5 and C8; and Specimens C6 and C9. Each pair consists of two different cross sections, but they were subjected to the same loading history and boundary conditions. Referring to Fig. 3, although all the test specimens developed their plastic flexural strength, the ones with the less-compact cross sections (i.e., W24×84) experienced rapid strength deterioration. For instance, Specimen C3 lost 80% of its flexural capacity at 5% rads [Fig. 3(c)], whereas Specimen C7 lost the same amount at 4% rads [Fig. 3(f)]. Referring to Figs. 4(e and h), at a reference drift of 4%, the W24×84 columns experienced approximately 20% more axial shortening because of severe web local buckling, compared to the W24×146 columns, regardless of the lateral-loading protocol or the loading direction. These results suggest that the current AISC (2010a) compactness limits for highly ductile members warrant further review such that the column flexural strength deterioration and axial shortening meet certain acceptance criteria at a reference lateral drift amplitude.

Referring to Figs. 3(e and h), at a reference story-drift ratio of 4%, the unloading stiffness of Specimens C6 and C9 was reduced by more than 40 and 70%, respectively, with respect to their initial elastic stiffness. Referring to Table 1, the W24×84 columns have a relatively large member slenderness ($L_b/r_y = 79$) and torsional

slenderness ratio ($\lambda_{LTB} = 0.42$) compared to the W24×146 specimens. This makes them more susceptible to out-of-plane and torsional deformations. For instance, at a story-drift ratio of 4%, Specimen C9 experienced approximately double the out-of-plane deformations near its column base compared to Specimen C6. This observation also holds true for the other two pairs of specimens. These results suggest that an upper limit on the member and torsional slenderness ratios should be used in future versions of the AISC (2010a) provisions for the collapse prevention of steel SMFs subjected to low probability of occurrence earthquakes.

Effect of Column End Boundary Conditions

Referring to Figs. 3(a and c), although the differences in the deduced moment-rotation relations of nominally identical specimens with fixed-fixed [Specimen C1, see Fig. 3(a)] and fixed-flexible [Specimen C3, see Fig. 3(c)] boundary conditions are practically negligible, the column axial shortening of the former [Fig. 4(a)] is nearly double than that of the latter [Fig. 4(c)]. This is attributed to the simultaneous formation of local buckling at both ends of a fixed-end column. In this case, the member loses its torsional (J) and warping resistance (C_w) simultaneously at both ends. This is not representative of typical first-story steel columns in capacity-designed steel MRFs. Fig. 10(a) shows a comparison of the deduced moment-plastic rotation relation at the column top for Specimens C1 and C3. To facilitate the comparison, both moment-rotation relations are plotted up to the second cycle of the 4% drift amplitude (Fig. 3). Because of the flexible top end, Specimen C3 experienced a maximum plastic rotation of 1% rads because flexural yielding occurred at its top end only after the 3% drift amplitude of the lateral-loading protocol used. The inelastic deformation at the top of Specimen C3 is attributed to the increased flexural demands at the same location once local buckling forms and progresses near the column base.

The proper representation of the member end boundary conditions has potential implications on the expected steel column unloading stiffness deterioration under reversed cyclic loading. In particular, Fig. 10(b) shows a comparison of the unloading stiffness to the initial elastic stiffness ratio for Specimens C1 and C3 with respect to the peak drift amplitudes of a symmetric cyclic loading protocol. Up to 3% drift, the unloading stiffness deterioration of Specimen C1 is more than double compared to that of Specimen C3. This is primarily due to the simultaneous loss of the torsional restraint in fixed-end columns, such as in Specimen C1. In particular, Specimen C1 experienced twisting angles (θ_z) almost two times larger than those observed in Specimen C3. From Fig. 10(b), at 4% drift, representative of low probability of occurrence earthquakes, Specimen C1 (fixed-fixed) underpredicts the rate of unloading stiffness deterioration compared to Specimen C3 (fixed-flexible). This is attributed to the fact that the weak-axis bending demands, triggered by the large out-of-plane deformations because of in-plane bending, are not adequately captured in fixed-end columns [Fig. 8(c)]. In fact, Specimen C1 experienced 40% less out-of-plane deformations compared to Specimen C3.

At drift ratios less than 3%, fixed-flexible specimens, including those with $L_b/r_y = 79$, did not experience significant twisting. These findings contradict recent observations from Ozkula et al. (2017) that specimens with even lower member slenderness $L_b/r_y \approx 70$ experienced lateral torsional buckling at similar lateral drift demands. This indicates that (a) the expected failure modes in steel columns may be fairly misleading if fixed-fixed boundary conditions are considered; and (b) the current CSA S16-09 seismic provisions may be fairly conservative by limiting $L_b/r_y \approx 60$ for

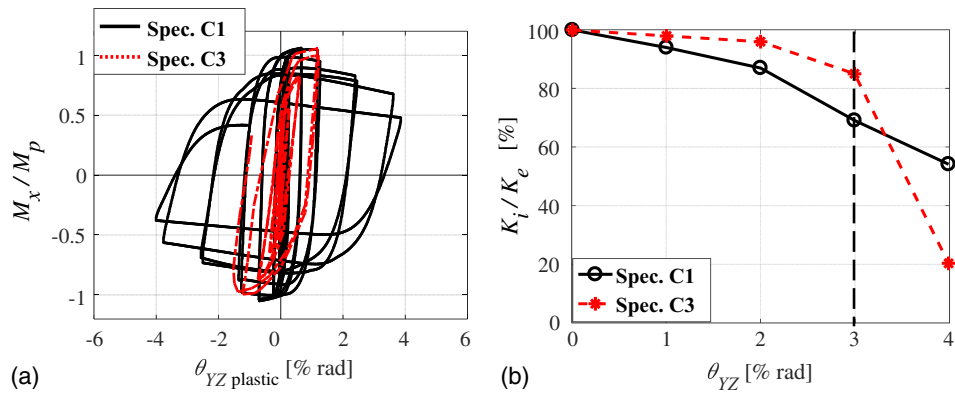


Fig. 10. Specimens C1 (fixed-fixed boundary conditions) and C3 (fixed-flexible boundary conditions): (a) column top end moment versus plastic rotation; (b) normalized unloading stiffness at peak drift amplitudes

Type-D steel MRFs; hence, this limit could be revisited in future editions.

Effect of Compressive Axial Load

The effect of the applied compressive axial load on the column stability is evaluated by comparing the hysteretic behavior of Specimens C1 ($P/P_y = 0.2$) and C2 ($P/P_y = 0.5$). Both specimens were subjected to a symmetric lateral-loading protocol. Referring to Figs. 3(a and b), it is evident that when the applied compressive axial load increases, the rate of cyclic and in-cycle flexural strength deterioration of the column increases considerably; therefore, its plastic deformation capacity decreases. This agrees with prior studies (MacRae et al. 1990; Ozkula et al. 2017). Notably, Fig. 3(b) indicates that Specimen C2 was still able to develop an appreciable plastic rotational capacity even though $P/P_{c1} > 50\%$. Therefore, this member should not be treated as a force-controlled element as per ASCE-41-13 (ASCE 2014). This has direct implications for the seismic retrofit of existing tall buildings in which steel columns with stocky cross sections are treated as force-controlled elements if $P/P_{c1} > 50\%$ (Bech et al. 2015).

Referring to Fig. 4(a), Specimen C1 shortened minimally ($\delta_z = 0.6\%L$) at 2% drift compared to Specimen C2, which shortened by $4\%L$ [Fig. 4(b)] at the same drift amplitude. This was due to severe web and flange local buckling in the presence of high compressive axial load demands. This suggests that in modern capacity-designed steel-frame buildings with MRFs, an upper limit on the axial compressive load demands should be set. For instance, the seismic provisions in New Zealand (SNZ 2007) limit the compressive axial load demands to $50\%P_y$ for Category 1 (i.e., highly ductile) column members. The Canadian seismic provisions (CSA 2009) prohibit the use of $P/P_y > 30\%$ in steel columns as part of Type-D ductile steel MRFs. The test results and a corroborating parametric finite-element analysis study (Elkady and Lignos 2015a; Elkady 2016) suggest that the latter limit seems to be more rational. Notably, the AISC (2010a) seismic provisions and the steel specification (AISC 2010b) do not impose such a limit.

Effect of Lateral-Loading Sequence

Representative first-cycle envelope curves are shown in Fig. 11 for three pairs of nominally identical specimens subjected to the two different lateral-loading histories: Specimens C3 and C5; Specimens C7 and C8; and Specimens C9 and C10. From this figure, for drifts up to approximately 2% (i.e., drifts associated with service- or design-basis seismic events), the lateral-loading protocol

used does not practically affect the first-cycle envelope curve of a steel column. This is important if the objective is to evaluate the immediate occupancy of a steel-frame building after a design-basis seismic event. On the other hand, for drifts larger than 2%, specimens subjected to a symmetric lateral-loading protocol deteriorate much faster in flexural strength than those subjected to a collapse-consistent loading history. In particular, the plastic deformation capacity of steel columns subjected to the latter protocol is twice larger than that of nominally identical columns subjected to the former (Fig. 11). This is attributed to the extent of inelastic cumulative damage because of the relatively large number of inelastic cycles of a symmetric cyclic loading history.

Interestingly, from Fig. 4, at 4% drift, test specimens subjected to a collapse-consistent loading protocol shortened, on average, by $0.6\%L$. This is five times less than the average amount of axial shortening measured in nominally identical columns subjected to a symmetric cyclic loading history (i.e., $2.7\%L$). Therefore, experimental data from symmetric loading histories would be overly conservative for the performance-based seismic evaluation of steel-frame buildings subjected to low probability of occurrence earthquakes.

In brief, the aforementioned facts underscore the importance of using realistic loading histories for the calibration of component deterioration models used for the earthquake-induced collapse assessment of frame buildings. Such protocols should capture the ratcheting behavior that a building and its structural components experience prior to structural collapse. These findings are in agreement with past collapse-related studies (FEMA 2009; Krawinkler 2009; Lignos et al. 2011; Suzuki and Lignos 2014, 2015).

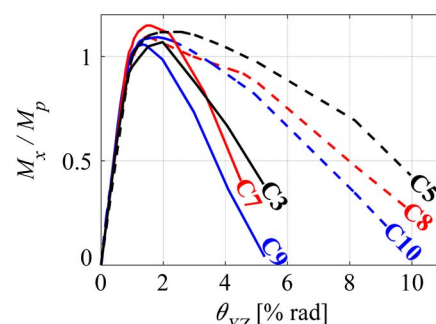


Fig. 11. First-cycle envelopes for all specimens with fixed-flexible boundary conditions subjected to symmetric cyclic (solid lines) and collapse-consistent loading protocols (dashed lines)

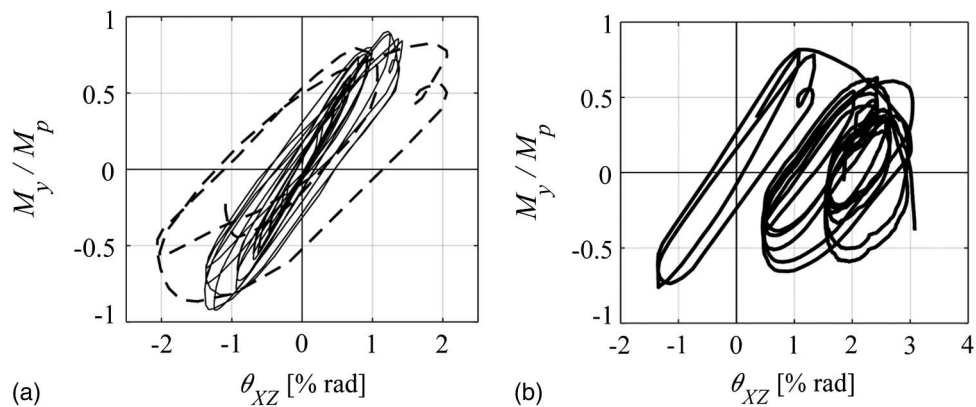


Fig. 12. Normalized column base weak-axis moment versus true chord rotation in the weak-axis direction: (a) Specimen C6; (b) Specimen C10

Effect of Bidirectional Lateral Loading

The experimental program offers the opportunity to characterize the hysteretic behavior of steel columns subjected to bidirectional lateral loading coupled with compressive axial load and further assess their performance with respect to nominally identical specimens subjected to unidirectional lateral loading. Referring to Fig. 3, three pairs of specimens are compared for this purpose; Specimens C3 and C6; Specimens C7 and C9; and Specimens C8 and C10. From this figure, for all practical purposes, the rate of flexural strength deterioration as well as the plastic deformation capacity of the examined steel columns are not influenced by the bidirectional loading especially prior to the 3% drift amplitude in the column's strong-axis bending direction, regardless of the cross section used and the lateral-loading history. At larger drifts, the observed differences in the column's flexural strength deterioration are on the order of 15% or less. These differences are primarily attributed to the generally larger out-of-plane deformations measured in the plastic hinge region near the column base of the specimens that experienced a bidirectional lateral loading [Fig. 8(b)] compared to those that experienced unidirectional loading [Fig. 8(a)].

Representative deduced moment-rotation relations with respect to the weak axis of steel columns are shown in Figs. 12(a and b) for Specimens C6 and C10, respectively. In Fig. 12(a), the moment-rotation behavior following the onset of local buckling at the column base is highlighted with a dashed line. From Fig. 12(a), up to an approximate 2% drift in the weak-axis orientation, the hysteretic behavior of Specimen C6 is fairly stable without any observed weak-axis flexural strength deterioration. Referring to Fig. 12(b), Specimen C10 exhibited appreciable cyclic flexural strength deterioration in the weak-axis bending direction. This is due to the fairly large inelastic cycles that this column experienced in the same loading direction (i.e., 3% drift amplitude).

Referring to Fig. 3, if the objective is to develop simplified backbone component models for the nonlinear modeling of steel columns in line with ASCE-41-13 (ASCE 2014), no adjustments are needed for a steel column's plastic deformation capacity because of the bidirectional loading. This effect is only reflected in the column's flexural strength because of axial load-bidirectional bending interaction ($P-M_x-M_y$). With reference to Figs. 4(g and i), at a given drift amplitude in the strong-axis orientation, the amount of column axial shortening is practically not influenced by the bidirectional loading. Same findings hold true regardless of the cross section used.

The test results suggest that specimens subjected to bidirectional loading developed the center of local buckling farther away from the column base compared to those subjected to unidirectional

loading. For example, the center of local buckling was located at $0.7d$ from the column base for Specimen C10 compared to $0.4d$ for Specimen C8. This is attributed to the member P-delta demands about the column's weak axis in the case of bidirectional loading.

Steel columns subjected to bidirectional lateral loading experienced larger out-of-plane deformations compared to those subjected to unidirectional lateral loading. This observation was more evident in W24×84 columns (e.g., Specimens C7 and C9) at story drifts larger than 3% [Figs. 8(a and b)]. These specimens are more susceptible to out-of-plane instabilities because of their larger member slenderness ratio (L_b/r_y) and torsional slenderness ratio (λ_{LTB}) compared to W24×146 columns (Table 1). This caused the unloading stiffness of Specimen C9 to deteriorate more than that of Specimen C7 [Figs. 3(f and h)].

Column Plastic Hinge Length and Comparisons with Available Empirical Equations

The column plastic hinge length, L_{PH} , was systematically evaluated for all the test specimens based on the uniaxial strain gauge measurements recorded along their height. Referring to Fig. 13, L_{PH} is defined as the distance between the column base and the cross section at which the uniaxial engineering strain exceeds the measured engineering yield strain, ε_y . From the same figure, this location is traced by conducting a linear interpolation between the engineering strain measurements at cross-section level #2 (ε_{2-2}), which is located at 305 mm (12 in.) from the column base, and cross-section level #3 (ε_{3-3}), which is located at 1,270 mm (50 in.) from the column base. Representative L_{PH} evolutions for four specimens subjected to various loading histories are shown in Fig. 14. In this figure, L_{PH} is normalized with respect to the cross-section depth, d . From this figure, prior to the onset of local

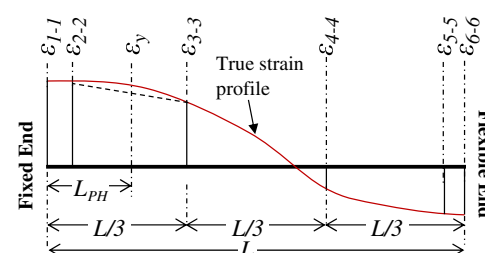


Fig. 13. Plastic hinge length computation using strain gauge measurements

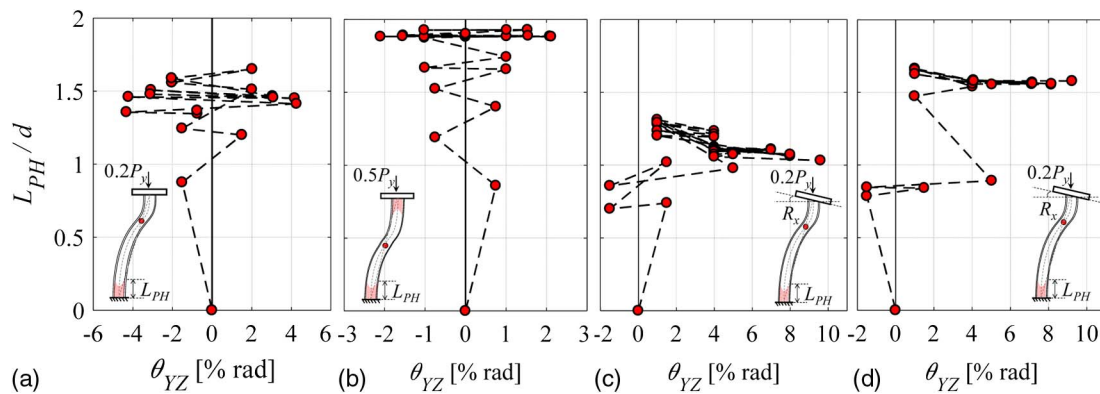


Fig. 14. Plastic hinge length at peak drifts versus true chord rotation for selected specimens: (a) Specimen C3 (W24×146, SYM-UD-0.2Py); (b) Specimen C1 (W24×146, SYM-UD-0.5Py); (c) Specimen C8 (W24×84, CPS-UD-0.2Py); (d) Specimen C10 (W24×84, CPS-BD-0.2Py)

buckling near the column base, the progression of L_{PH} is due to the cyclic hardening of the steel material. This becomes evident for the more compact cross sections [Figs. 14(a and b)] because of the delayed onset of local buckling. Referring to Fig. 14, after the local buckling formation, the plastic hinge length stabilizes because of the localization of plastic strains within the buckled region. This is confirmed in Fig. 15, which shows the normalized L_{PH} for all the tested specimens at the end of each test and that at a reference story drift of 2%, local buckling did not occur in most cases.

Referring to Figs. 14(a and b), when the applied compressive axial load increases, the plastic hinge length becomes larger. In particular, Specimen C2 developed a 15% larger plastic hinge length compared to Specimen C1. This is due to the second-order moment that pushes the maximum moment demands (i.e., first- and second-order moment) farther away from the column base. This was also observed in specimens subjected to bidirectional lateral loading [Fig. 14(d)]. In this case, the weak-axis bending demands because of the out-of-plane deformations are larger compared to those subjected to unidirectional loading [Fig. 14(c)].

Referring to Fig. 15, Specimens C1–C6, which used a W24×146 cross section, developed a plastic hinge length in the range of 1.6–1.9 d regardless of the lateral-loading history and the member's end boundary conditions. These values are in agreement with the current seismic provisions in New Zealand (SNZ 2007), which specify a minimum plastic hinge length of 1.5 d for Category 1 and 2 members (equivalent to highly ductile and moderately ductile members as per AISC (2010a)). On the other hand, Specimens C7–C10, which used a W24×84 cross section, developed a plastic hinge length in the range of 1.25–1.85 d . Notably, SNZ (2007) specifies a lower minimum plastic hinge length of 1.0 d for Category 3 members [i.e., equivalent to

noncompact cross sections as per AISC (2010a)]. Similar to SNZ (2007), the plastic hinge length may be used to evaluate the steel column stability requirements in terms of the cross-section restraint spacing, against out-of-plane deformations and twisting, within the member's yielded regions. A similar approach may be adopted in future revisions of the current North American seismic provisions for steel MRFs (CSA 2009; AISC 2010a).

The expected plastic hinge lengths of the test specimens are calculated based on the empirical equation developed by Kemp (1996) as follows:

$$L_{PH} = 0.067 \left(\frac{60}{\lambda_{eff}} \right)^{1.5} L_i \quad \text{where } \lambda_{eff} = k_f k_w k_d \left(\frac{L_i}{r_{yc}} \right) \gamma, \\ \gamma = \sqrt{\frac{F_y (\text{MPa})}{250}}, \quad k_f = \left(\frac{b_f}{2t_f} \right) \frac{\gamma}{9}, \quad k_w = \left(\frac{h_w}{t_w} \right) \frac{\gamma}{70} \\ k_d = 1.0, \text{ for bare steel beams} \quad (1)$$

where L_i = distance from the cross section with the maximum flexural strength to the nearest inflection point; and r_{yc} = radius of gyration of the compressive region. The L_{PH} values computed by Eq. (1) were, on average, equal to 1.67 and 1.54 d for W24×146 and W24×84 columns, respectively. Referring to Fig. 15, these values are fairly close to the average ones obtained from the measurements of the two groups of specimens (i.e., less than 5% difference). Note that Eq. (1) is applicable to cross sections with $5 < b_f/2t_f < 11$ and $39 < h/t_w < 85$. The cross sections that were used in the test program fall into this range. Although it is difficult to generalize the experimental findings because the tests cover only a limited range of local slenderness ratios, it seems that Kemp's equation can be used to estimate the plastic hinge length of steel columns that use slender cross sections near the current compactness limits for highly ductile and moderately ductile members according to AISC (2010); however, this finding should be further verified for stockier members. The authors are currently evaluating this issue through parametric finite-element analyses (Elkady and Lignos 2015a, 2017).

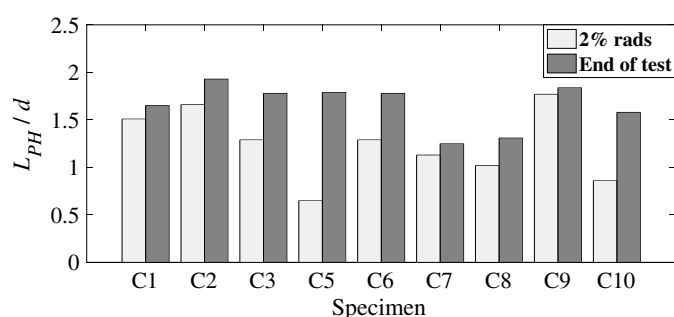


Fig. 15. Progression of plastic hinge length at selected drift amplitudes

Column Axial Shortening and Comparisons with Available Predictive Equations

Column axial shortening is typically neglected in column stability checks in North America. It directly relates to the cumulative plastic rotation ($\sum \theta_{pl}$) that a member experiences during reversed cyclic loading (MacRae et al. 1990), which in turn depends on the lateral-loading history. Fig. 16 shows the measured amount

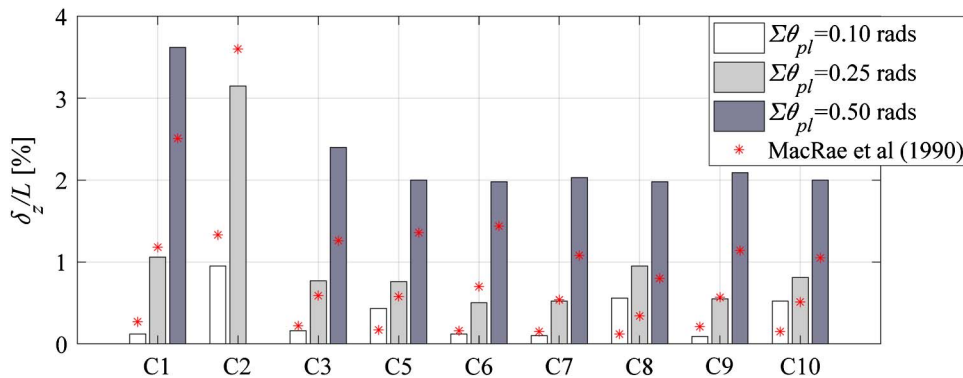


Fig. 16. Normalized column axial shortening at different levels of cumulative plastic rotation

of axial shortening for all the specimens at selected $\sum\theta_{pl}$ values of 0.1, 0.25, and 0.5 rads. To put these values into perspective, they correspond roughly to the amount of cumulative plastic rotation measured at the first cycle of 1, 2, and 4% drift amplitudes of an equivalent symmetric cyclic loading protocol. In the context of this paper, $\sum\theta_{pl}$ is computed by assuming an elastically perfect plastic hysteretic behavior and a yield rotation $\theta_y = Z_x f_{ye} (1 - P/P_y)/K_e$ (where Z_x = plastic section modulus; and f_{ye} = expected yield stress of the steel material). From Fig. 16, at $\sum\theta_{pl} < 0.25$ rads (i.e., equivalent to 2% drift), nominally identical specimens experience the same amount of axial shortening at a given cumulative plastic rotation regardless of the lateral-loading protocol used (i.e., collapse-consistent versus symmetric cyclic and/or bidirectional versus unidirectional). In particular, column axial shortening is less than 1% of the member length, L , at $\sum\theta_{pl} < 0.25$ rads. Therefore, it should not become a controlling issue for design-basis seismic events (i.e., 10% probability of occurrence in 50 years). However, column axial shortening grows exponentially at $\sum\theta_{pl} \approx 0.50$ rads (i.e., equivalent to 4% drift). Therefore, this failure mode could become controlling for collapse prevention during seismic events with low probability of occurrence (i.e., 2% probability of occurrence over 50 years).

MacRae et al. (1990) used the experimental data from small-scale cantilever column testing to develop an empirical equation to estimate the amount of column axial shortening (Δ_{axial}) as follows:

$$\Delta_{axial} = 0.446 \frac{P}{2.54P_y} \frac{A}{A_w} L_{PH} \sum \theta_{pl}$$

$$\text{for } \frac{P}{P_y} \leq \frac{2.54A_w}{A} = 0.446 L_{PH} \sum \theta_{pl} \quad \text{for } \frac{P}{P_y} > \frac{2.54A_w}{A} \quad (2)$$

where A_w = web area; A = gross area; and L_{PH} = column plastic hinge length. The computed column axial shortening for all 10 specimens based on Eq. (2) is superimposed in Fig. 16 for the three values of $\sum\theta_{pl} = 0.1, 0.25$, and 0.5 rads. For these calculations, the assumed plastic hinge length, L_{PH} , is equal to the measured values for each specimen (Fig. 15). For fixed-end columns (i.e., Specimens C1 and C2), the calculated axial shortening was multiplied by a factor of two to account for the simultaneous formation of plastic hinges at the member ends. Referring to Fig. 16, Eq. (2) seems to reasonably predict the axial shortening of columns subjected to a symmetric lateral-loading protocol (i.e., C1, C2, C3, C6, C7, and C9), at cumulative plastic rotations of 0.25 rads or less. In this range, the relation $\Delta_{axial} - \sum\theta_{pl}$ is fairly linear as implied by Eq. (2); however, if $\sum\theta_{pl} > 0.25$, Eq. (2) significantly underestimates the column axial shortening. This is due to its exponential

increase with local buckling progression (Elkady and Lignos 2015a). This issue should be further considered in future studies.

Lateral Stability Bracing Force Demands and Comparisons with Commonly Used Equations for Predicting Strength of Nodal Brace Axial Forces

The six-DOF test setup offers the opportunity to measure the lateral stability bracing forces acting at the top end of a column specimen under unidirectional lateral loading. To the best of the authors' knowledge, the lateral stability bracing force demands have not been evaluated experimentally in prior studies. In that respect, the experimental data set is considered to be unique.

Fig. 17 shows representative lateral stability bracing force demands, F_x , versus the true chord rotation for six specimens. The out-of-plane force is normalized with respect to P_y . From Fig. 17, W24×146 and W24×84 columns developed, on average, a maximum out-of-plane force of 1.5% P_y and 0.8% P_y , respectively, at their top end. As L_b/r_y increases, the out-of-plane deformations near the plastic hinge region of a steel column increase; therefore, no significant out-of-plane forces are exerted at the column top end, regardless of the lateral-loading protocol used.

Section 6.4 of ANSI/AISC 360-10 (AISC 2010b) specifies that the required nodal brace axial force strength, P_{rb} , shall be determined as the sum of the beam bracing axial force and beam-column bracing axial force as follows:

$$P_{rb} = 0.01P_r + 0.02M_r C_d/h_o \quad (3)$$

where P_r and M_r = column's required axial and flexural strength, respectively; $C_d = 2.0$ for braces closest to the column inflection point; and h_o = distance between the flange centroids. Similarly, Clause 9.2.5 of CSA (2009) specifies a lateral brace axial strength, P_b , larger than 2% of the factored compressive force, C_f , of the element being braced laterally as follows:

$$P_b = 0.02C_f = 0.02 \times 1.1 \times f_{ye} A_{comp} \quad (4)$$

where f_{ye} = expected yield stress; and A_{comp} = cross-sectional area subjected to compressive stresses. The out-of-plane force demands that were measured during the testing program are used to assess the adequacy of the brace design axial forces calculated by Eqs. (3) and (4). These forces are calculated and superimposed in Fig. 17. In Eq. (3), P_r is assumed to be equal to the applied compressive axial load ratio to the corresponding specimen; and M_r is assumed to be equal to the reduced plastic flexural strength based on the AISC (2010b) P - M interaction equations. In Eq. (4), A_{comp} is calculated by assuming that 65 and 100% of the cross-section depth is under

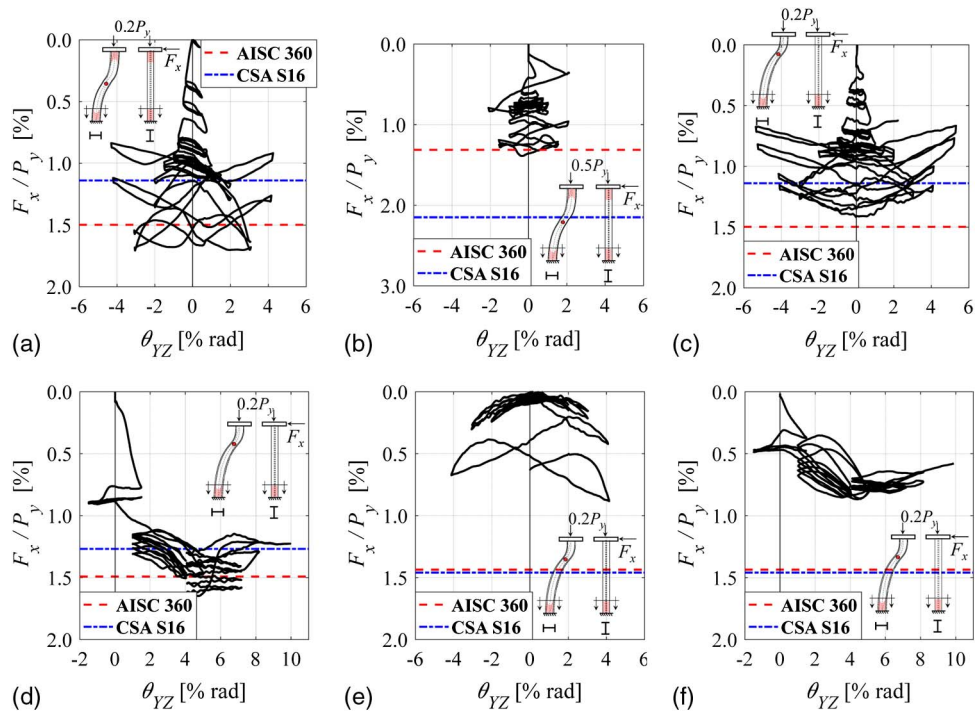


Fig. 17. Measured lateral stability bracing force demands at column top end versus true chord rotation for selected specimens: (a) Specimen C1 (W24×146); (b) Specimen C2 (W24×146); (c) Specimen C3 (W24×146); (d) Specimen C5 (W24×146); (e) Specimen C7 (W24×84); (f) Specimen C8 (W24×84)

compression when subjected to 20% P_y and 50% P_y , respectively. These values were estimated from a stress distribution that was obtained once flexural yielding was initiated in the respective cross section. Referring to Fig. 17, the lateral brace design axial force as per CSA (2009) and AISC (2010b) for the W24×146 columns seems adequate for story-drift ratios up to approximately 2%; however, at larger drift demands, the lateral stability bracing force demands exceed the lateral bracing design axial force based on Eqs. (3) and (4) by 35 and 15%, respectively. On the other hand, the lateral brace design force seems fairly conservative for all the W24×84 columns regardless of the lateral-loading history and the corresponding lateral drift demands. These observations suggest that the lateral brace design axial force requirements for steel columns in MRFs should be carefully revisited.

Summary and Conclusions

This paper presents findings and design implications based on 10 full-scale tests of deep and slender (with local slenderness near the AISC 341-10 λ_{hd} limits) W24 (i.e., 600-mm deep) first-story steel columns subjected to various cyclic loading histories. The test specimens represent interior first-story steel columns in capacity-designed steel MRFs. Several key parameters, including the member end boundary conditions, loading sequence, and local web and member slenderness, are interrogated. The effects of bidirectional versus unidirectional lateral-loading histories were also examined by conducting tests on nominally identical specimens. The lateral-loading histories were either symmetric cyclic or collapse consistent such that ratcheting prior to structural collapse was considered. The main findings are summarized as follows:

- Qualitatively, the test specimens with fixed-flexible boundary conditions followed a similar damage progression. Web and flange local buckling (at displacements corresponding to 1.5–2% story drift) formed at a distance of 0.5–0.7 d from the column

base. Subsequently, local buckling caused column axial shortening, which in turn triggered out-of-plane deformations that became maximum at the center of the plastic hinge region near the column base. The out-of-plane deformations caused considerable weak-axis bending demands because of member P-delta effects. Notably, these deformations were not evident in fixed-end test specimens. The out-of-plane deformations were often followed by twisting at drifts larger than 3%. The twist angle magnitude is dependent on the member and torsional slenderness ratios.

- The experimental program suggests that it may be fairly misleading to characterize the hysteretic behavior of steel columns under multiaxis loading with simplified fixed-fixed boundary conditions. In this case, the torsional restraint at both member ends is lost simultaneously after the onset of local buckling, which is not typical for first-story columns in capacity-designed steel MRFs because of the strong-column/weak-beam ratio used, and therefore, member geometric instabilities are more likely to occur at fairly small lateral drifts compared to reality. For instance, at story drifts up to 3% rads, test specimens with $L_b/r_y = 79$ and fixed-flexible boundary conditions were able to maintain 80% of their maximum flexural strength as well as 70% of their elastic stiffness. The same specimens experienced minimal twisting up to this drift range.
- The tests suggest that the current CSA S16-09 (CSA 2009) standards may be fairly conservative by setting an $L_b/r_y \approx 60$ limit for the steel column design in Type-D steel MRFs [i.e., equivalent to SMFs according to the AISC (2010a) provisions]. A modified upper limit for the member and torsional slenderness ratios should be adopted in future versions of the CSA (2009) and AISC (2010a) provisions for collapse prevention of SMFs. This requires additional research studies.
- Axial shortening is a controlling failure mode in steel columns undergoing reversed cyclic loading. At story drifts representative of design-basis earthquakes (i.e., 2% rads), axial shortening

ranged from 0.3 to 0.5% L for specimens subjected to a compressive axial load of 20% P_y ; however, a W24×146 column subjected to 50% P_y experienced 2.5%– L axial shortening at the same drift ratio. This indicates that an upper limit should be set to the allowable compressive axial load for the seismic design of steel columns in steel SMFs in future revisions of the AISC (2010) provisions. In that respect, the 30% P_y limit that was used according to the Canadian seismic provisions (CSA 2009) for ductile steel MRFs seems to be rational.

- The tests reveal that the column axial shortening is strongly dependent on the cumulative plastic rotation. This agrees with MacRae et al. (1990). MacRae's column axial shortening predictive empirical equation seems adequate for drift ratios up to 2%. In this range, column axial shortening is linearly dependent on the cumulative plastic rotation. In the examined cases herein, the same equation seems to underpredict the column axial shortening by more than 50% at drifts larger than 2%. In this drift range, the axial shortening increases exponentially with respect to the cumulative plastic rotation; this is due to the rapid progression of web local buckling in the plastic hinge region.
- A W24×146 steel column subjected to a symmetric cyclic loading history coupled with a $P/P_y = 50\%$ (i.e., $P/P_{c1} > 50\%$) developed an appreciable plastic deformation capacity prior to the loss of its axial load-carrying capacity. Although inconclusive, this suggests that the ASCE/SEI 41-13 (ASCE 2014) recommendations for force-controlled elements may be fairly conservative. This issue should be examined in future studies.
- The plastic deformation of steel columns subjected to a collapse-consistent loading protocol was at least twice larger than those subjected to a symmetric cyclic loading protocol. Notably, at drifts larger than 4%, steel columns subjected to a collapse-consistent loading protocol shortened five times less than those subjected to a symmetric loading protocol. These findings underscore the importance of using realistic loading histories for characterizing the "ratcheting" hysteretic behavior (drifting in one direction) of structural components from the onset of damage through structural collapse.
- The test results suggest that steel columns subjected to bidirectional lateral loading develop the center of the local buckling wave farther away from the column base compared to those subjected to unidirectional lateral loading. This is due to the increased weak-axis flexural demands because of the weak-axis lateral drift as well as the increased member P-delta. These effects were more pronounced for W24×84 columns in which $L_b/r_y = 79$; however, if the objective is to develop simplified backbone component models for nonlinear modeling of steel columns to conduct a nonlinear static analysis of steel MRFs, no adjustments are necessary to the plastic deformation capacity of steel columns due to bidirectional lateral loading.
- The developed plastic hinge length near the column base was in the range of 1.25–1.85 d for W24×84 columns. Stockier W24×146 columns developed, on average, a larger plastic hinge length of 1.6–1.9 d because of material cyclic hardening prior to the onset of geometric instabilities. These values are fairly consistent with the ones reported in the New Zealand seismic provisions for the design of steel MRFs (SNZ 2007). It was found that the empirical equation developed by Kemp (1996) can be used to estimate the expected plastic hinge length of steel columns that use slender cross sections near the current compactness limits for highly ductile and moderately ductile members according to AISC (2010). This conclusion should be verified for stockier members in future studies.
- Comparisons of measured and calculated lateral stability bracing force demands in steel columns generally confirm

expectations only for the stockier W24×146 columns ($L_b/r_y = 51$ and $\lambda_{LTB} = 0.28$) up to story drifts of 2% or less, regardless of the lateral-loading protocol used. At larger drift demands, the lateral stability bracing force demands exceeded the lateral bracing design axial force according to the CSA (2009) and AISC (2010b) specifications by 15 and 35%, respectively, for the same cross sections. On the other hand, the calculated lateral brace design force seems to be fairly conservative for all the W24×84 columns ($L_b/r_y = 79$ and $\lambda_{LTB} = 0.42$) regardless of the corresponding lateral drift demands and the lateral-loading history.

Acknowledgments

This study is based on work supported by the National Science and Engineering Research Council of Canada (NSERC) under the Discovery Grant Program. The Steel Structures Education Foundation (SSEF) also provided funding for the testing program. Funding is also provided by the Swiss National Science Foundation (Award No. 200021_169248). The financial support is gratefully acknowledged. ADF Corporation, Inc. donated the material fabrication for four of the specimens. The authors would like to sincerely thank Prof. Robert Tremblay, École Polytechnique de Montréal (EPM), for providing the opportunity to use the unique six-DOF test setup and resources at EPM. The authors sincerely thank the technical staff at the EPM structures laboratory for their invaluable assistance during the testing program. Any opinions, findings, and conclusions or recommendations expressed in this paper are those of the authors and do not necessarily reflect the views of sponsors.

References

- AISC. (2010a). "Seismic provisions for structural steel buildings." *ANSI/AISC 341-10*, Chicago.
- AISC. (2010b). "Specification for structural steel buildings." *ANSI/AISC 360-10*, Chicago.
- ASCE. (2014). "Seismic evaluation and retrofit of existing buildings." *ASCE/SEI 41-13*, Reston, VA.
- ASTM. (2014). "Standard specification for general requirements for rolled structural steel bars, plates, shapes, and sheet piling." *ASTM A6/A6M-14*, West Conshohocken, PA.
- ASTM. (2015). "Standard specification for structural steel shapes." *ASTM A992/A992M-11*, West Conshohocken, PA.
- Bech, D., Tremayne, B., and Houston, J. (2015). "Proposed changes to steel column evaluation criteria for existing buildings." *Proc., 2nd ATC-SEI Conf. on Improving the Seismic Performance of Existing Building and Other Structures*, Earthquake Engineering Research Institute, San Francisco.
- Chi, B., and Uang, C.-M. (2002). "Cyclic response and design recommendations of reduced beam section moment connections with deep columns." *J. Struct. Eng.*, 10.1061/(ASCE)0733-9445(2002)128:4 (464), 464–473.
- Clark, P., Frank, K., Krawinkler, H., and Shaw, R. (1997). "Protocol for fabrication, inspection, testing, and documentation of beam-column connection tests and other experimental specimens." *Rep. No. SAC-BD-97/02*, FEMA, Washington, DC.
- CSA (Canadian Standards Association). (2009). "Design of steel structures." *CAN/CSA S16-09*, Mississauga, Canada.
- Elkady, A. (2016). "Collapse risk assessment of steel moment resisting frames designed with deep wide-flange columns in seismic regions." Ph.D. thesis, McGill Univ., Montreal.
- Elkady, A., and Lignos, D. G. (2012). "Dynamic stability of deep slender steel columns as part of special MRFs designed in seismic regions: Finite element modeling." *Proc., 1st Int. Conf. on Performance-Based and Life-Cycle Structural Engineering (PLSE)*, Hong Kong Polytechnic Univ., Hong Kong.

Elkady, A., and Lignos, D. G. (2013). "Collapse assessment special steel moment resisting frames members deep with designed." *Proc., Vienna Congress on Recent Advances in Earthquake Engineering and Structural Dynamics (VEESD)*, Austrian Association for Earthquake Engineering and Structural Dynamics, Vienna Univ. of Technology, Vienna, Austria.

Elkady, A., and Lignos, D. G. (2014). "Modeling of the composite action in fully restrained beam-to-column connections: Implications in the seismic design and collapse capacity of steel special moment frames." *J. Earthquake Eng. Struct. Dyn.*, 43(13), 1935–1954.

Elkady, A., and Lignos, D. G. (2015a). "Analytical investigation of the cyclic behavior and plastic hinge formation in deep wide-flange steel beam-columns." *Bull. Earthquake Eng.*, 13(4), 1097–1118.

Elkady, A., and Lignos, D. G. (2015b). "Effect of gravity framing on the overstrength and collapse capacity of steel frame buildings with perimeter special moment frames." *J. Earthquake Eng. Struct. Dyn.*, 44(8), 1289–1307.

Elkady, A., and Lignos, D. G. (2017). "Stability requirements of deep steel wide-flange columns under cyclic loading." *Proc., ASCE Annual Stability Conf.*, ASCE, Reston, VA.

FEMA. (2000). *State of the art report on connection performance*, Washington, DC.

FEMA. (2009). *Effects of strength and stiffness degradation on the seismic response of structural systems*, Washington, DC.

Fogarty, J., and El-Tawil, S. (2015). "Collapse resistance of steel columns under combined axial and lateral loading." *J. Struct. Eng.*, 10.1061/(ASCE)ST.1943-541X.0001350, 04015091.

Galambos, T. V., and Surovek, A. E. (2008). *Structural stability of steel: Concepts and applications for structural engineers*, Wiley, New York.

Gupta, A., and Krawinkler, H. (1999). "Seismic demands for the performance evaluation of steel moment resisting frame structures." *Rep. No. 132*, Stanford Univ., Stanford, CA.

Ibarra, L. F., and Krawinkler, H. (2005). "Global collapse of frame structures under seismic excitations." *Rep. No. 152*, Stanford Univ., Stanford, CA.

Kemp, A. R. (1996). "Inelastic local and lateral buckling in design codes." *J. Struct. Eng.*, 10.1061/(ASCE)0733-9445(1996)122:4(374), 374–382.

Krawinkler, H. (1996). "Cyclic loading histories for seismic experimentation on structural components." *Earthquake Spectra*, 12(1), 1–12.

Krawinkler, H. (2009). "Loading histories for cyclic tests in support of performance assessment of structural components." *Proc., 3rd Int. Conf. on Advances in Experimental Structural Engineering*, Pacific Earthquake Engineering Research Center, San Francisco.

Lignos, D. G., Hikino, T., Matsuoka, Y., and Nakashima, M. (2013). "Collapse assessment of steel moment frames based on E-Defense full-scale shake table collapse tests." *J. Struct. Eng.*, 10.1061/(ASCE)ST.1943-541X.0000608, 120–132.

Lignos, D. G., and Krawinkler, H. (2011). "Deterioration modeling of steel components in support of collapse prediction of steel moment frames under earthquake loading." *J. Struct. Eng.*, 10.1061/(ASCE)ST.1943-541X.0000376, 1291–1302.

Lignos, D. G., and Krawinkler, H. (2013). "Development and utilization of structural component databases for performance-based earthquake engineering." *J. Struct. Eng.*, 10.1061/(ASCE)ST.1943-541X.0000646, 1382–1394.

Lignos, D. G., Krawinkler, H., and Whittaker, A. S. (2011). "Prediction and validation of sidesway collapse of two scale models of a 4-story steel moment frame." *Earthquake Eng. Struct. Dyn.*, 40(7), 807–825.

Lignos, D. G., Zareian, F., and Krawinkler, H. (2010). "A steel component database for deterioration modeling of steel beams with RBS under cyclic loading." *Proc., ASCE Structures Congress*, ASCE, Orlando, FL, 1275–1286.

MacRae, G. A., Carr, A. J., and Walpole, W. R. (1990). "The seismic response of steel frames." Ph.D. thesis, Univ. of Canterbury, Christchurch, New Zealand.

MacRae, G. A., Urmon, C. R., Walpole, W. R., Moss, P., Hyde, K., and Clifton, C. (2009). "Axial shortening of steel columns in buildings subjected to earthquakes." *Bull. N. Z. Soc. Earthquake Eng.*, 42(4), 275–287.

Nakashima, M., Takanashi, K., and Kato, H. (1990). "Test of steel beam-columns subject to sidesway." *J. Struct. Eng.*, 10.1061/(ASCE)0733-9445(1990)116:9(2516), 2516–2531.

Newell, J. D., and Uang, C.-M. (2008). "Cyclic behavior of steel wide-flange columns subjected to large drift." *J. Struct. Eng.*, 10.1061/(ASCE)0733-9445(2008)134:8(1334), 1334–1342.

NIST (National Institute of Standards and Technology). (2010a). "Evaluation of the FEMA P695 methodology for quantification of building seismic performance factors." *Rep. No. NIST GCR 10-917-8*, Gaithersburg, MD.

NIST (National Institute of Standards and Technology). (2010b). "Research plan for the study of seismic behaviour and design of deep slender wide-flange structural steel beam-column members." *Rep. No. NIST GCR 11-917-13*, Gaithersburg, MD.

Ozkula, G., Harris, J., and Uang, C.-M. (2017). "Observations from cyclic tests on deep, wide- beam-column columns." *AISC Eng. J.*, 54(1), 45–61.

Popov, E. P., Bertero, V. V., and Chandramouli, S. (1975). "Hysteretic behavior of steel columns." *Rep. No. EERC 75-11*, Univ. of California, La Jolla, CA.

Ricles, J. M., Zhang, X., Fisher, J. W., and Lu, L. W. (2004). "Seismic performance of deep column-to-beam welded reduced beam section moment connections." *Proc., 5th Int. Workshop Connections in Steel Structures V: Behaviour, Strength, and Design*, American Institute of Steel Construction, Amsterdam, Netherlands, 211–222.

SNZ (Standards New Zealand). (2007). "Steel structures standard." *NZS 3404:2007*, Wellington, New Zealand.

Stoakes, C. D., and Fahnestock, L. A. (2016). "Strong-axis stability of wide-flange steel columns in the presence of weak-axis flexure." *J. Struct. Eng.*, 10.1061/(ASCE)ST.1943-541X.0001448, 04016004.

Suzuki, Y., and Lignos, D. G. (2014). "Development of loading protocols for experimental testing of steel columns subjected to combined high axial load and lateral drift demands near collapse." *Proc., 10th National Conf. on Earthquake Engineering*, Earthquake Engineering Research Institute, Anchorage, AK.

Suzuki, Y., and Lignos, D. G. (2015). "Large scale collapse experiments of wide-flange steel beam-columns." *Proc., 8th Int. Conf. on Behavior of Steel Structures in Seismic Areas (STESSA)*, Tongji Univ., Shanghai, China.

Zhang, X., and Ricles, J. M. (2006). "Experimental evaluation of reduced beam section connections to deep columns." *J. Struct. Eng.*, 10.1061/(ASCE)0733-9445(2006)132:3(346), 346–357.